ACS APPLIED MATERIALS & INTERFACES

Research Article

www.acsami.org

Self Powered Highly Enhanced Dual Wavelength ZnO@CdS Core–Shell Nanorod Arrays Photodetector: An Intelligent Pair

Sanjit Sarkar and Durga Basak*

Department of Solid State Physics, Indian Association for the Cultivation of Science, Jadavpur, Kolkata-700032, India

ABSTRACT: On the face of the impending energy crisis, developing low-energy or even zero-energy photoelectronic devices is extremely important. A multispectral photosensitivity feature of a self-powered device provides an additional powerful tool. We have developed an unprecedented high performance dual wavelength self-powered ZnO@CdS/PEDOT:PSS core–shell nanorods array photodetector through a simple aqueous chemical method wherein a suitable band alignment between an intelligent material pair, i.e. ZnO and CdS, has been utilized. Besides a noteworthy advantage of the devices being that they show a very sharp and prominent dual wavelength photosensitivity, both the ultraviolet and visible light sensitivity (ratio of current under illumination (I_{photo})/current under dark (I_{dark})) of the device are two orders of higher magnitude than those of pristine ZnO, attaining values of 2.8×10^3 and 1.07×10^3, respectively. At the same time, temporal responses faster than 20 ms could be achieved with these solution-processed photodetectors. The present study provides a very important direction to engineer core–shell nanostructured devices for dual wavelength high photosensitivity.

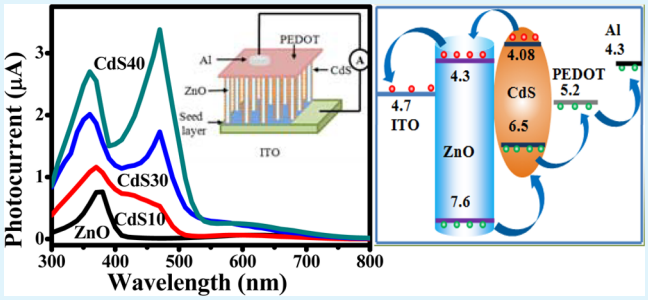

KEYWORDS: *self-powered, ZnO, hybrid nanostructures, photodetector, dual wavelength*

INTRODUCTION

One dimensional (1D) ZnO nanostructures have drawn tremendous attention of the research community due to their efficient and potential applications in nanoscale optoelectronic devices, such as nanoscale lasers, light-emitting diodes, photovoltaic (PV) cells, and ultraviolet (UV) photodetectors.[1−13] In particular, single crystal ZnO nanostructures (nanorods, nanowires, nanowalls, and nanoparticles) are ideal formations for UV photodetectors with high responsivities and fast recovery times, as compared to thin film or bulk-based detectors.[14−17] Thus, in the past few years, a considerable number of studies have been carried out, with a main focus on utilizing nanoengineered 1D ZnO nanostructures for further enhancing the UV photodetection property. In typical ZnO-based photodetectors, a bias voltage is required to separate the photogenerated charge carriers, which enhances the conductivity and hence the photoresponsivity.[14,18−22] In recent years it has been realized that few ZnO-based hybrid nanosystems can show a photoresponse without any external bias rendering the devices as self-powered.[23−25] 1D ZnO nanostructures based self-powered photodiodes have been reported based on the photovoltaic behavior of the device.[23,26−29] Bie and co-workers[29] reported a visible-blind GaN/ZnO NWs-based p−n junction that gives a photocurrent of 2 μA under zero bias at a high irradiance power of 100 W cm^{-2} with growth and decay time constants of 20 and 219 μs, respectively. The ZnO-reduced graphene oxide heterojunction based self-powered photodetector has shown a photocurrent of 0.09 μA for a low irradiation power of 80 mW with a growth time constant of 0.2 s.[23] While, more recently, Yang et al.[30] have reported a photocurrent of 14 μA with high irradiance power of 8 W for ZnO nanorods/polyaniline heterostructures with the growth and decay times of the order of second. A photocurrent gain of 10^3 with a response time of the order of second has been observed for the ZnO/PEDOT:PSS based p−n junction by illuminating the sample with a 325 nm laser source.[31] A relatively lower and slower response at higher irradiance power has been cited in most of the above-mentioned studies although the majority of the practical applications require higher performance. For example, environmental monitoring and medical therapy treatment require weak and rapid light detection besides the advantage of zero power input. Therefore, due to insignificant progress in this new field of self-powered photodetectors to date, considerable future study on fabrication and characterization is needed.

Recently, there has been a great deal of interest in the fabrication of multispectral photodetectors for various applications, such as discrimination of objects, imaging under varying atmospheric conditions, etc.[32] In particular, the UV and visible dual wavelength operation is very attractive for applications such as broad wavelength emission detection and environmental and biological research.[25] In order to get a response in several wavelength regions, one approach is to assemble several stacks of square quantum wells with different

Received: April 13, 2015
Accepted: July 8, 2015
Published: July 8, 2015

DOI: 10.1021/acsami.5b03184
ACS Appl. Mater. Interfaces 2015, 7, 16322−16329

peak response wavelengths.[33,34] The other approach is to build a heterostructured junction of dissimilar energy gaps. Obviously the latter is much simpler. However, it is difficult to achieve both the features of dual wavelength detection and self-powering in a single device structure, and thus, logically only a couple of self-powered ZnO-based multispectral photoresponsive devices have been reported recently by Zhan et al.[23] and Game et al.[25] using ZnO-reduced grapheme oxide and N doped ZnO/spiro-MeOTAD heterostructures, respectively. In both the studies, the visible photoresponse has been achieved by exploiting the below band gap trap states present in ZnO, although the selectivity for visible light is poor, as reported by Game et al.[25] It is quite evident that as the visible responsivity in those junctions has been acquired at the expense of UV responsivity, both responsivities are not likely to be augmented at the same time, since the number of photogenerated carriers is constant. Thus, achieving both UV and visible photoresponsivity high in ZnO-based devices remains a big challenge to overcome. Along these lines, to remove the present problems of improving the detecting parameters, optimizing the trade-off between responsivity and speed, and spectra engineering, a heteronanojunctioned ZnO-based dual wavelength photodetector has been developed by us, keeping in mind the fact that a suitable band alignment may enhance both the detection efficiencies. To the best of our knowledge, in this paper, we report for the first time an unprecedented high performance of a dual wavelength self-powered ZnO@CdS core−shell nanorods' (NRs) array photodetector fabricated through a simple aqueous chemical method wherein an intelligent material pair, i.e. ZnO and CdS, has been utilized. We have demonstrated a way to achieve dual wavelength photodetection with very fast response and high photosensitivity at as low as incident power of 1 mW for UV and 2 mW for visible light. Additionally, the photodetector shows very sharp wavelength selectivity.

EXPERIMENTAL METHODS

ZnO NRs were synthesized by aqueous chemical growth (ACG) method as described earlier.[35] In brief, a solution of zinc acetate ($(CH_3COO)_2Zn{\cdot}2H_2O$) and hexamethylenetetramine ($(CH_2)_6N_4$) (10 mM) in deionized water was prepared as the precursor and was taken in a beaker, placed on a hot plate at 90 °C. Preseeded ITO substrates were placed at the bottom of the beaker for the growth of ZnO NRs. After the growth, the substrate was taken out of the beaker, rinsed with deionized water and dried at 90 °C for further characterization. The CdS shell on the ZnO NRs was grown by SILAR method. In this method, ZnO NRs were successively immersed in aqueous solution of cadmium acetate ($Cd(CH_3CO_2)_2$) and thioacetamide (C_2H_5NS) followed by immersion in deionized water to remove the excess ion. To achieve different shell thickness, the process was repeated for 10, 30, 40 times. After the coating, substrates were rinsed with water and dried at 90 °C for further characterization. Next, PEDOT:PSS was spin coated on ITO/ZnO@CdS as hole transporting layer. Finally, Al metal contact was deposited on PEDOT:PSS by thermal evaporation through mechanical mask of diameter 1 mm. The heterojunctions were named as CdS10, CdS30 and CdS40 wherein the CdS coating was done for 10, 30, and 40 times, respectively. The schematic of the device structure is shown in Figure 1(a). For a control experiment, only CdS layer has been grown by the following method: at first ZnO seed layer was deposited on ultrasonically cleaned ITO. Then the seed layer was transformed to ZnS by dipping in aqueous solution of thioacetamide at 90 °C and then to CdS layer by dipping successively in aqueous solution of $Cd(CH_3CO_2)_2$, water, thioacetamide and water respectively for 20 s each. The process is repeated for 30 times.

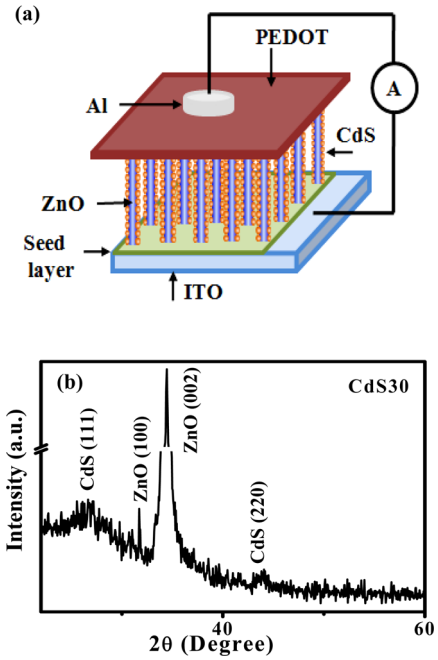

Figure 1. (a) Schematic of the device. (b) XRD pattern of a representative sample CdS30.

The structural confirmation was obtained using Bruker X-ray diffractometry (model: D8). The microstructural analyses were done by field emission scanning electron microscopy (FESEM model JEOL JSM-6700F) and field emission gun transmission electron microscopy (FEGTEM; model JEOL JEM 2010). The currents were measured using a Keithley source meter (model 2400) when the sample was kept in the dark as well as under illumination by the light from a xenon lamp (model no. 66902) fitted with a monochromator. All the measurements were performed at room temperature.

RESULTS AND DISCUSSIONS

The X-ray diffraction pattern of a representative sample, CdS30, illustrated in Figure 1(b), shows two peaks at 2θ = 31.7 and 34.4° which have been identified as the (100) and (002) peak of the wurtzite structure of ZnO, confirmed from the JCPDS data (File no. CDF 92-1A-APR 93). Two humps have been observed at 2θ = 28 and 44.5°, which are assigned respectively to the (111) and (220) peaks of hexagonal CdS nanoparticles[36] by comparing with JCPDS data. The morphologies of the ZnO@CdS NRs arrays have been revealed in Figure 2. NRs with a clear hexagonal tip of diameter ∼40−50 nm are seen for a pristine ZnO sample (Figure 2(a)) while the hexagonal tips are found to be covered with nanoparticles for the CdS10 sample (Figure 2(b)). In this case, the diameter is increased to ∼50−60 nm due to nanoparticle segregation onto the NRs. The FESEM image for the CdS30 sample in Figure 2(c) shows that the NRs' surfaces are covered with a lot of nanoparticles and the hexagonal shape of the tip has been changed to a rounded one with a diameter of ∼70−80 nm. In the case of the CdS40 sample, the top view of the NRs' array is changed to a granular filmlike morphology wherein each granule's diameter is ∼80−90 nm. The thickness of the shell layer thus has been estimated from the FESEM images to be around 5, 15, and 20 nm, respectively, for 10, 30, and 40 times CdS coatings. The TEM and HRTEM images of pristine ZnO, respectively, in Figure 3(a) and 3(b) confirm the diameter of a NR to be 45−50 nm and show lattice fringes of width 0.26 nm corresponding to the (0002) plane of the wurtzite structure of

DOI: 10.1021/acsami.5b03184
ACS Appl. Mater. Interfaces 2015, 7, 16322−16329

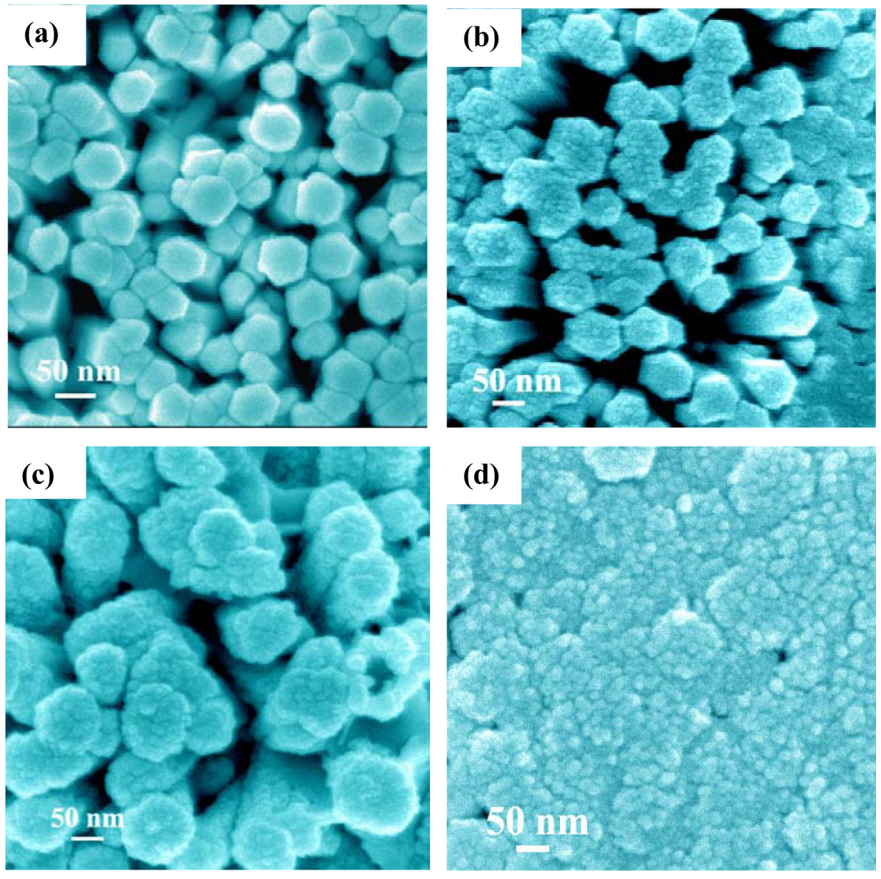

Figure 2. FESEM images of the samples. (a) ZnO, (b) CdS10, (c) CdS30, and (d) CdS40.

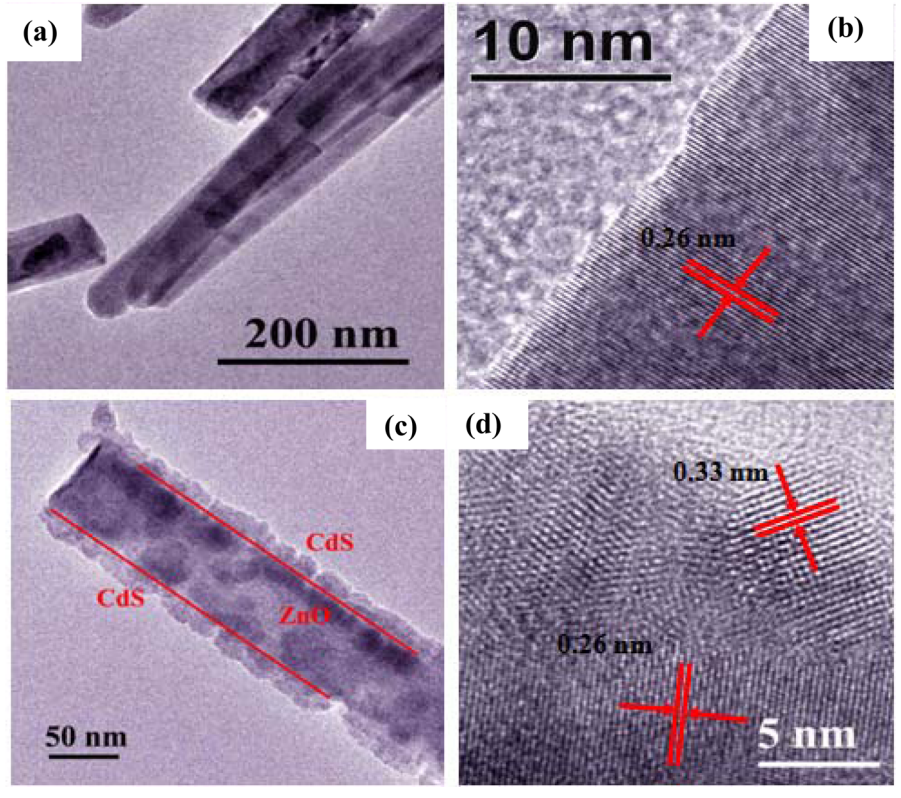

Figure 3. TEM image of ZnO (a), HRTEM image of ZnO (b), TEM image of CdS30 (c), and HRTEM image of CdS30 (d).

DOI: 10.1021/acsami.5b03184
ACS Appl. Mater. Interfaces 2015, 7, 16322−16329

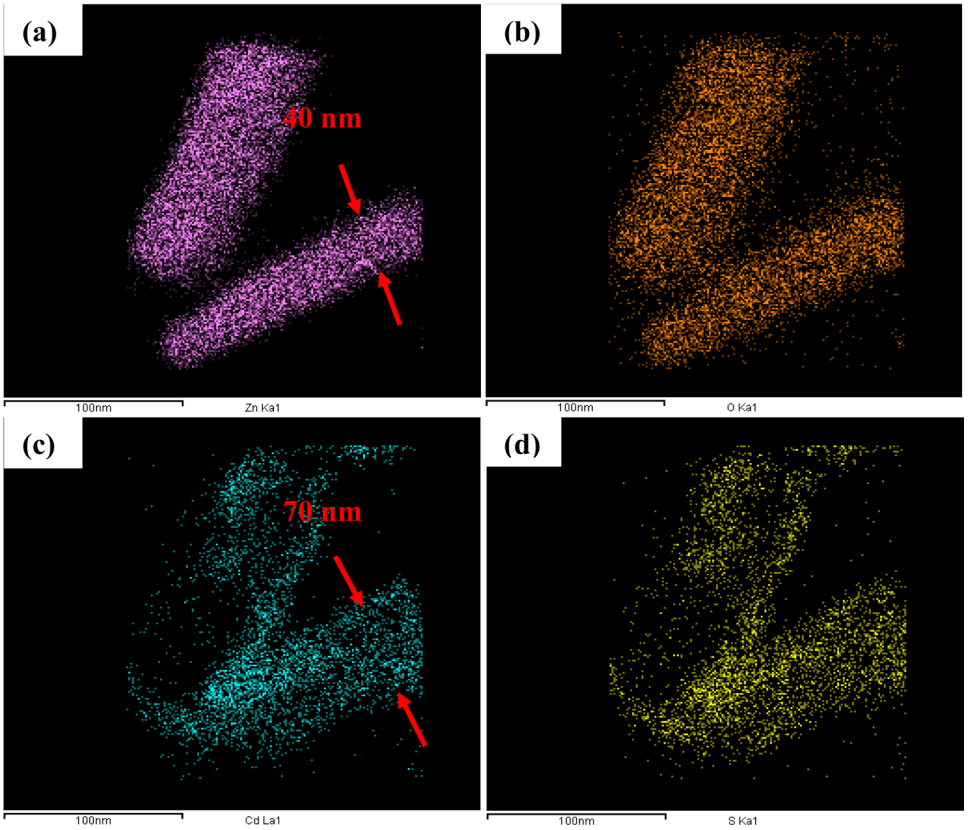

Figure 4. Elemental mapping of the representative sample CdS30. (a), (b), (c), and (d) Mapping of the elements Zn, O, Cd, and S, respectively.

ZnO. Figure 3(c) and 3(d) show the typical TEM and HRTEM images of the CdS30 sample as a representative of the ZnO@CdS series. The figure clearly demonstrates a shell layer of thickness ∼13−15 nm around a ZnO NR which is supported by the FESEM image also (Figure 2(c)). The HRTEM image in Figure 3(d) shows lattice fringes of two different dimensions: the ones in the core of 0.26 nm width corresponding to the (0002) plane of wurtzite ZnO and the ones in the shell of 0.33 nm width corresponding to the (111) plane of CdS. Further confirmation for the ZnO@CdS core−shell structure for CdS30 is obtained from the elemental mapping, as revealed in Figure 4(a−d). These clearly show that Zn and O elements are present in the core for a width of ∼40 nm while Cd and S elements are present in the shell for a width of ∼15 nm, which is in excellent agreement with the FESEM and TEM images.

I−*V* characteristics under dark conditions for all the samples in Figure 5(a) show rectifying behavior which confirms formation of the p−n junction in the ZnO@CdS/PEDOT:PSS device structure. The rectification ratio increases with an increase in the shell thickness (Table 1) due to better passivation of the ZnO surface, resulting in lower leakage current.[37,38] The dark and photo *I*−*V* characteristics of a representative sample, CdS30, are presented in Figure 5(b). Enhanced currents clearly indicate that the device is responsive to both UV and visible light. The inset of Figure 5(b) further shows that under zero bias condition the device is responsive to both UV and visible light, indicating performance of the device in self-powered mode. The photovoltages of the representative sample CdS30 under UV and visible illumination have been measured to be 0.15 and 0.06 V, respectively. The power conversion efficiency also has been calculated and found to be 0.32 and 0.03% for UV and visible illuminations, respectively.

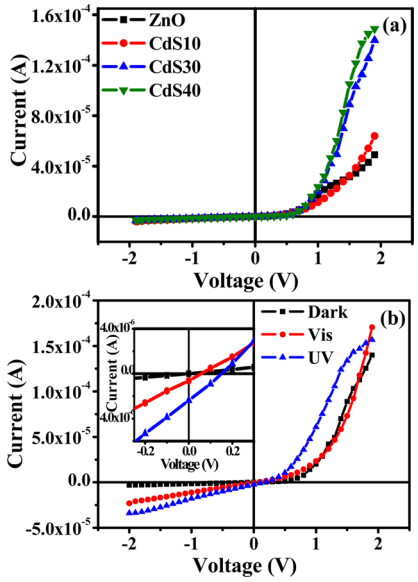

Figure 5. (a) *I*−*V* characteristics of the samples. (b) *I*−*V* characteristics of the representative samples under dark, UV light, and visible light illumination. Inset of (b) shows the magnified view of *I*−*V* curves around zero bias.

The photocurrent spectra of all the samples under zero bias are shown in Figure 6(a). The pristine ZnO shows no significant increase in the photocurrent in the entire visible region but shows a sharp rise in the current at around 400 nm. For ZnO@CdS samples, as the CdS layer thickness increases, the photocurrent increases both in the UV as well as in the 500−400 nm region, resulting in two sharp peaks for CdS30

DOI: 10.1021/acsami.5b03184
ACS Appl. Mater. Interfaces 2015, 7, 16322−16329

Table 1. Forward Current (I_F), Reverse Current (I_R), and Rectification Ratio (I_F/I_R) of All the Samples under Dark

sample name	I_F at +2 V (A)	I_R at −2 V (A)	I_F/I_R
ZnO	4.89×10^{-5}	3.52×10^{-6}	14
CdS10	6.38×10^{-5}	3.91×10^{-6}	16
CdS30	1.4×10^{-4}	3.05×10^{-6}	46
CdS40	1.5×10^{-4}	2.93×10^{-6}	51

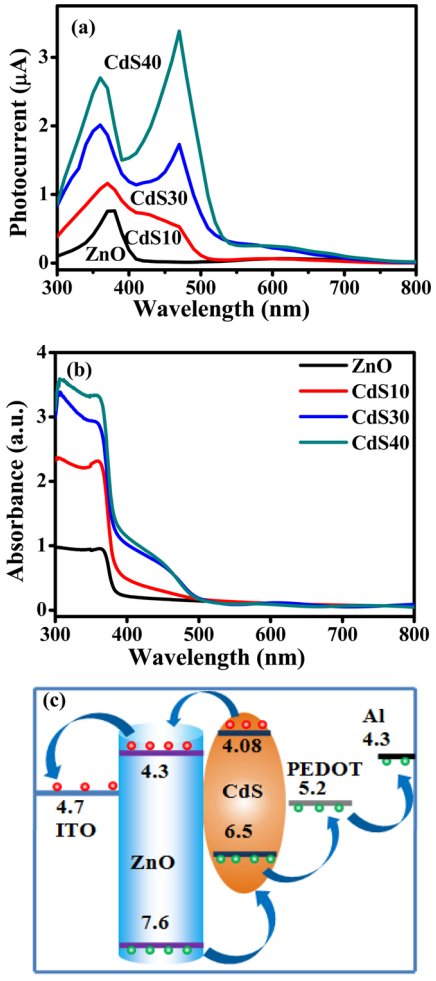

Figure 6. (a) Photocurrent spectra of the samples. (b) Absorbance spectra of the samples. (c) Band diagram of the device showing the charge transfer mechanism.

and CdS40 in the said regions. This indicates that the device can efficiently perform as a dual wavelength photodetector. However, Game et al.[25] and Zhan et al.[23] have not shown any spectral dependence of their devices. The spectral selectivity Q_λ (ratio of the photocurrent at a certain wavelength λ to the photocurrent at 800 nm) has been calculated for all the samples from the photocurrent spectra. The value Q_{370} increases from 37 for ZnO to 2.23×10^2 for CdS30 and to 2.0×10^2 for the CdS40 sample. On the other hand, Q_{470} increases from 7 for ZnO to 1.8×10^2 for CdS30 and to 2.6×10^2 for the CdS40 sample. Maximum spectral selectivity for the visible light occurs when the CdS thickness is maximum (CdS40), which can be explained by the absorbance spectra of the samples and the band diagram of the device. The absorption spectra of the samples in Figure 6(b) show that the absorbance in the region 400−500 nm increases with an increase in the CdS layer coating, which is quite expected. A similar absorption spectrum was observed by Tak et al.[39] for CdS nanoparticle/ZnO nanowires arrays. From the band diagram (Figure 6(c)), it is clear that, by absorbing the visible light, photogenerated electrons from the CB of CdS can be easily transferred to ZnO and then to ITO for the suitable band alignment. Also the holes in the VB of CdS can be transferred to PEDOT:PSS and then to the Al electrode, resulting in high visible photocurrent. By absorbing the UV light, the photogenerated electrons from the CB of ZnO are easily transferred to ITO and holes from the VB of ZnO to Al via CdS and PEDOT:PSS. Therefore, maximum spectral selectivity for the UV light occurs for CdS30, which is due to optimum absorption of UV light and surface passivation of ZnO due to the CdS layer. So in the case of visible light detection, ZnO acts as electron transporting layer and CdS acts as light absorbing material. On the other hand, in the case of UV light detection, ZnO acts as light absorbing material and CdS acts as electron blocking and hole transporting layer. Thus, the separations of the photogenerated carriers in both CdS and ZnO efficiently occurred due to suitable band alignments.

The transient photoresponse curves under zero bias for all the samples have been shown in Figure 7(a and b). The dark

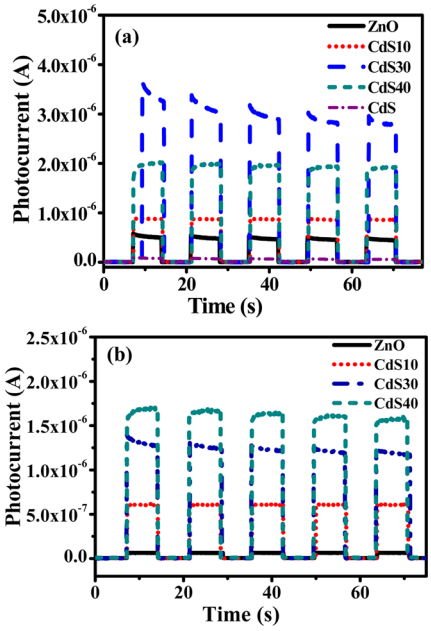

Figure 7. Transient response of the photocurrent under zero bias voltage: (a) under UV light, (b) under 470 nm light.

current, photocurrent, and photoconductive gain of all the samples are shown in Table 2. The dark current value for only ZnO is 6.4×10^{-9} A which is due to the surface defects. However, the value decreases as more and more CdS is coated. This is because of ZnO NRs' surface passivation by the CdS layer. Under UV light, all the samples show very fast growth and decay of the photocurrents. The photocurrent value increases with an increase in the shell thickness up to CdS30, beyond which the photocurrent decreases slightly. This decrease might be due to the shielding of some UV light by the CdS layer. The UV ON/OFF ratio increases from a value of 90 for pristine ZnO to a value of 2.8×10^3 for the CdS30 sample, which means a more than two order enhancement in the UV photoresponse in the core/shell sample has been noticed. The UV response of only the pristine CdS sample is

DOI: 10.1021/acsami.5b03184
ACS Appl. Mater. Interfaces 2015, 7, 16322−16329

Table 2. Dark Current, Photocurrent, and Responsivity of the Samples at Zero Bias Voltage

sample name	dark current I_{dark} (A)	UV photocurrent I_{UV} (A)	visible photocurrent $I_{visible}$ (A)	UV response (I_{UV}/I_{dark})	visible response ($I_{visible}/I_{dark}$)
ZnO	6.4×10^{-9}	5.70×10^{-7}	6.43×10^{-8}	89	10
CdS10	4.4×10^{-9}	8.86×10^{-7}	6.03×10^{-7}	2.01×10^{2}	1.37×10^{2}
CdS30	1.3×10^{-9}	3.65×10^{-6}	1.40×10^{-6}	2.80×10^{3}	1.07×10^{3}
CdS40	1.9×10^{-9}	2.00×10^{-6}	1.69×10^{-6}	1.05×10^{3}	8.89×10^{2}

very low, as shown in Figure 7(a). Therefore, this enhanced UV response is mainly due to two reasons: (1) Surface modification of ZnO by CdS through passivation of the defect states and (2) Electron blocking by the CdS layer. A thin layer of CdS over ZnO NRs passivates the surface defect states of ZnO, which in turn enhances the carrier lifetime. Hence, the carrier separation increases.[40,41] Our UV photoresponse value (2.8×10^3 at a power of 1 mW/cm^2) is much higher than the values obtained by Zhan et al.[23] (~100 at a power of 80 mW), Lin et al.[31] (10^3, power is not mentioned), and Game et al.[25] (300 at a power of 3 mW/cm^2), which clearly shows that as a self-powered multispectral photodetector, our ZnO@CdS/PEDOT:PSS device shows a much higher performance for a lower incident power of UV light. The device shows similar behavior under 470 nm visible light, as shown in Figure 7(b). The ON/OFF ratio increases from a value of 10 for pristine ZnO to a value of 1.07×10^3 for CdS30, indicating a two order enhancement due to efficient separation of the photogenerated carriers in CdS via ZnO. Our visible photorespone value (1.07×10^3 at an incident power of 2 mW) is similar to the value reported by Game et al.[25] (1.6×10^3 at an incident power of 18 mW/cm^2) but is much higher than those reported by Zhan et al.[23] (430 at an incident power of 80 mW/cm^2). Thus, our results indicate that our core/shell NRs array photodetectors are much more efficient under both UV and visible illumination as compared to the reported self-powered multispectral photodetectors to date.

To further asses the efficiency of the devices, we have taken a deep look at the transient response curve of CdS30 as a representative sample (Figure 8(a and b)). The 100% photocurrent growth and decay times under UV illumination are measured to be equal or less than 20 and 40 ms, respectively, and they fall within the minimum resolution of our instrument. For visible light illumination, both growth and decay times are equal to or less than 20 ms. The response times of our devices are very fast and are of similar order as those reported by Game et al. (4 and 10 ms)[25] and much lower than those reported by Zhan et al. (200 ms)[23] and Lin et al. (1 s).[31]

To evaluate the stability of the device, we have performed the transient photoresponse measurements under UV light for 30 consecutive cycles, and the result is shown in Figure 8(c). It is clear from the figure that, up to 30 cycles, there is no significant change in the photocurrent due to UV illumination. Thus, we may conclude that our device is quite stable under UV illumination.

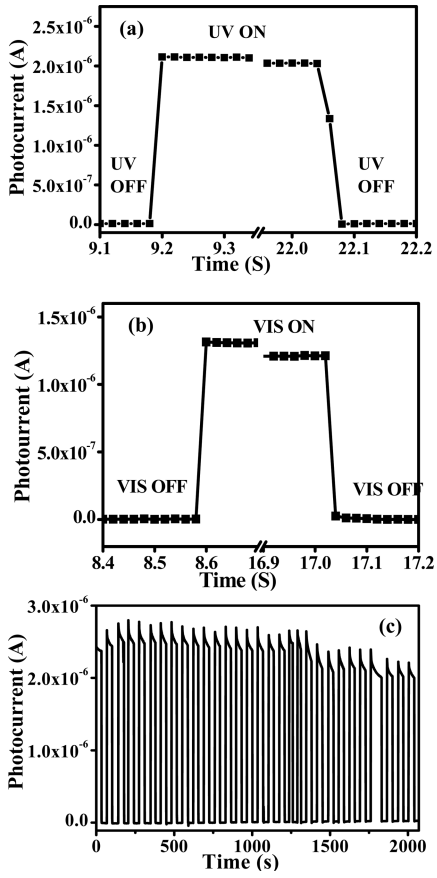

Figure 8. 100% growth and decay time of the representative sample CdS30: (a) under UV light, (b) under visible light. (c) The stability of a representative device up to 30 cycles.

CONCLUSIONS

In summary, we have developed ZnO@CdS/PEDOT:PSS core−shell NRs array photodetetor devices showing the self-powered UV and visible photoresponses two orders magnitude higher as compared to ZnO, only with response time constants equal to or less than 20 ms. Suitable band alignment between a ZnO and CdS pair in conjunction with PEDOT:PSS has led to an unprecedented high performance dual wavelength photodetector due to ZnO NRs surface modification by CdS and efficient charge separation at the interface. The choice of an intelligent pair with suitable band matching will open a new window to design an efficient self-powered multispectral photodetector.

AUTHOR INFORMATION

Corresponding Author

*E-mail: sspdb@iacs.res.in (D. Basak).

Notes

The authors declare no competing financial interest.

ACKNOWLEDGMENTS

S.S. is thankful to CSIR, New Delhi, India, for providing a fellowship.

REFERENCES

(1) Law, M.; Greene, L. E.; Johnson, J. C.; Saykally, R.; Yang, P. D. Nanowire Dye-Sensitized Solar Cells. *Nat. Mater.* **2005**, *4*, 455−459.

(2) Chu, S.; Olmedo, M.; Yang, Z.; Kong, J. Y.; Liu, J. L. Electrically Pumped Ultraviolet ZnO Diode Lasers on Si. *Appl. Phys. Lett.* **2008**, *93*, 181106.

DOI: 10.1021/acsami.5b03184
ACS Appl. Mater. Interfaces 2015, 7, 16322−16329

(3) Briseno, A. L.; Holcombe, T. W.; Boukai, A. I.; Garnett, E. C.; Shelton, S. W.; Frechet, J. J. M.; Yang, P. D. Oligo- and Polythiophene/ZnO Hybrid Nanowire Solar Cells. *Nano Lett.* **2010**, *10*, 334−340.
(4) Chandiran, A. K.; Abdi-Jalebi, M.; Nazeeruddin, M. K.; Gratzel, M. Analysis of Electron Transfer Properties of ZnO and TiO_2 Photoanodes for Dye-Sensitized Solar Cells. *ACS Nano* **2014**, *8*, 2261−2268.
(5) Ghosh, R.; Dutta, M.; Basak, D. Self-Seeded Growth and Ultraviolet Photoresponse Properties of ZnO Nanowire Arrays. *Appl. Phys. Lett.* **2007**, *91*, 073108.
(6) Hou, Y. N.; Mei, Z. X.; Liang, H. L.; Ye, D. Q.; Gu, C. Z.; Du, X. L. Dual-Band MgZnO Ultraviolet Photodetector Integrated with Si. *Appl. Phys. Lett.* **2013**, *102*, 153510.
(7) Yu, W. L.; Zhang, H.; Fan, Z. X.; Zhang, J. H.; Wei, H. T.; Zhou, D.; Xu, B.; Li, F. H.; Tian, W. J.; Yang, B. Efficient Polymer/Nanocrystal Hybrid Solar Cells Fabricated from Aqueous Materials. *Energy Environ. Sci.* **2011**, *4*, 2831−2834.
(8) Wang, X. D.; Song, J. H.; Liu, J.; Wang, Z. L. Direct-Current Nanogenerator Driven by Ultrasonic Waves. *Science* **2007**, *316*, 102−105.
(9) Chen, R.; Ye, Q. L.; He, T. C.; Ta, V. D.; Ying, Y. J.; Tay, Y. Y.; Wu, T.; Sun, H. D. Exciton Localization and Optical Properties Improvement in Nanocrystal-Embedded ZnO Core-Shell Nanowires. *Nano Lett.* **2013**, *13*, 734−739.
(10) Li, G. P.; Chen, R.; Guo, D. L.; Wong, L. M.; Wang, S. J.; Sun, H. D.; Wu, T. Nanoscale Semiconductor-Insulator-Metal Core/Shell Heterostructures: Facile Synthesis and Light Emission. *Nanoscale* **2011**, *3*, 3170−3177.
(11) Bera, A.; Peng, H. Y.; Lourembam, J.; Shen, Y. D.; Sun, X. W.; Wu, T. A Versatile Light-Switchable Nanorod Memory: Wurtzite ZnO on Perovskite $SrTiO_3$. *Adv. Funct. Mater.* **2013**, *23*, 4977−4984.
(12) Liu, X. Y.; Shan, C. X.; Jiao, C.; Wang, S. P.; Zhao, H. F.; Shen, D. Z. Pure Ultraviolet Emission from ZnO Nanowire-Based p-n Heterostructures. *Opt. Lett.* **2014**, *39*, 422−425.
(13) Fan, M. M.; Liu, K. W.; Zhang, Z. Z.; Li, B. H.; Chen, X.; Zhao, D. X.; Shan, C. X.; Shen, D. Z. High-Performance Solar-Blind Ultraviolet Photodetector Based on Mixed-Phase ZnMgO Thin Film. *Appl. Phys. Lett.* **2014**, *105*, 011117.
(14) Soci, C.; Zhang, A.; Xiang, B.; Dayeh, S. A.; Aplin, D. P. R.; Park, J.; Bao, X. Y.; Lo, Y. H.; Wang, D. ZnO Nanowire UV Photodetectors with High Internal Gain. *Nano Lett.* **2007**, *7*, 1003−1009.
(15) Das, S. N.; Moon, K. J.; Kar, J. P.; Choi, J. H.; Xiong, J.; Lee, T. I.; Myoung, J. M. ZnO Single Nanowire-Based UV Detectors. *Appl. Phys. Lett.* **2010**, *97*, 022103.
(16) Jin, Y. Z.; Wang, J. P.; Sun, B. Q.; Blakesley, J. C.; Greenham, N. C. Solution-Processed Ultraviolet Photodetedtors Based on Colloidal ZnO Nanoparticles. *Nano Lett.* **2008**, *8*, 1649−1653.
(17) Ghosh, T.; Basak, D. Highly Efficient Ultraviolet Photodetection in Nanocolumnar RF Sputtered ZnO Films: A Comparison between Sputtered, Sol-Gel and Aqueous Chemically Grown Nanostructures. *Nanotechnology* **2010**, *21*, 375202.
(18) Shao, D. L.; Yu, M. P.; Sun, H. T.; Hu, T.; Lian, J.; Sawyer, S. High Responsivity, Fast Ultraviolet Photodetector Fabricated from ZnO Nanoparticle-Graphene Core-Shell Structures. *Nanoscale* **2013**, *5*, 3664−3667.
(19) Li, P. J.; Liao, Z. M.; Zhang, X. Z.; Zhang, X. J.; Zhu, H. C.; Gao, J. Y.; Laurent, K.; Leprince-Wang, Y.; Wang, N.; Yu, D. P. Electrical and Photoresponse Properties of an Intramolecular p-n Homojunction in Single Phosphorus-Doped ZnO Nanowires. *Nano Lett.* **2009**, *9*, 2513−2518.
(20) Sarkar, S.; Basak, D. Defect Controlled Ultra High Ultraviolet Photocurrent Gain in Cu-Doped ZnO Nanorod Arrays: De-Trapping Yield. *Appl. Phys. Lett.* **2013**, *103*, 041112.
(21) Wang, Z. X.; Zhan, X. Y.; Wang, Y. J.; Muhammad, S.; Huang, Y.; He, J. A Flexible UV Nanosensor Based on Reduced Graphene Oxide Decorated ZnO Nanostructures. *Nanoscale* **2012**, *4*, 2678−2684.
(22) Zhang, F.; Niu, S. M.; Guo, W. X.; Zhu, G.; Liu, Y.; Zhang, X. L.; Wang, Z. L. Piezo-Phototronic Effect Enhanced Visible/UV Photodetector of a Carbon-Fiber/ZnO-CdS Double-Shell Microwire. *ACS Nano* **2013**, *7*, 4537−4544.
(23) Zhan, Z. Y.; Zheng, L. X.; Pan, Y. Z.; Sun, G. Z.; Li, L. Self-Powered, Visible-Light Photodetector Based on Thermally Reduced Graphene Oxide-ZnO (RGO-ZnO) Hybrid Nanostructure. *J. Mater. Chem.* **2012**, *22*, 2589−2595.
(24) Hatch, S. M.; Briscoe, J.; Dunn, S. A Self-Powered ZnO-Nanorod/CuSCN UV Photodetector Exhibiting Rapid Response. *Adv. Mater.* **2013**, *25*, 867−871.
(25) Game, O.; Singh, U.; Kumari, T.; Banpurkar, A.; Ogale, S. ZnO(N)-Spiro-MeOTAD Hybrid Photodiode: An Efficient Self-Powered Fast-Response UV (Visible) Photosensor. *Nanoscale* **2014**, *6*, 503−513.
(26) Ni, P. N.; Shan, C. X.; Wang, S. P.; Liu, X. Y.; Shen, D. Z. Self-Powered Spectrum-Selective Photodetectors Fabricated from n-ZnO/p-NiO Core-Shell Nanowire Arrays. *J. Mater. Chem. C* **2013**, *1*, 4445−4449.
(27) Hatch, S. M.; Briscoe, J.; Sapelkin, A.; Gillin, W. P.; Gilchrist, J. B.; Ryan, M. P.; Heutz, S.; Dunn, S. Influence of Anneal Atmosphere on ZnO-Nanorod Photoluminescent and Morphological Properties with Self-Powered Photodetector Performance. *J. Appl. Phys.* **2013**, *113*, 204501.
(28) Bai, Z. M.; Yan, X. Q.; Chen, X.; Liu, H. S.; Shen, Y. W.; Zhang, Y. ZnO Nanowire Array Ultraviolet Photodetectors with Self-Powered Properties. *Curr. Appl. Phys.* **2013**, *13*, 165−169.
(29) Bie, Y. Q.; Liao, Z. M.; Zhang, H. Z.; Li, G. R.; Ye, Y.; Zhou, Y. B.; Xu, J.; Qin, Z. X.; Dai, L.; Yu, D. P. Self-Powered, Ultrafast, Visible-Blind UV Detection and Optical Logical Operation Based on ZnO/GaN Nanoscale p-n Junctions. *Adv. Mater.* **2011**, *23*, 649−653.
(30) Yang, S. X.; Gong, J.; Deng, Y. L. A Sandwich-Structured Ultraviolet Photodetector Driven Only by Opposite Heterojunctions. *J. Mater. Chem.* **2012**, *22*, 13899−13902.
(31) Lin, P.; Yan, X. Q.; Zhang, Z.; Shen, Y. W.; Zhao, Y. G.; Bai, Z. M.; Zhang, Y. Self-Powered UV Photosensor Based on PEDOT:PSS/ZnO Micro/Nanowire with Strain-Modulated Photoresponse. *ACS Appl. Mater. Interfaces* **2013**, *5*, 3671−3676.
(32) Ariyawansa, G.; Apalkov, V.; Perera, A. G. U.; Matsik, S. G.; Huang, G.; Bhattacharya, P. Bias-Selectable Tricolor Tunneling Quantum Dot Infrared Photodetector for Atmospheric Windows. *Appl. Phys. Lett.* **2008**, *92*, 111104.
(33) Zhang, Y. H.; Jiang, D. S.; Xia, J. B.; Cui, L. Q.; Song, C. Y.; Zhou, Z. Q.; Ge, W. K. A Voltage-Controlled Tunable Two-Color Infrared Photodetector Using GaAs/AlAs/GaAlAs and GaAs/GaAlAs Stacked Multiquantum Wells. *Appl. Phys. Lett.* **1996**, *68*, 2114−2116.
(34) Tidrow, M. Z.; Chiang, J. C.; Li, S. S.; Bacher, K. A High Strain Two-Stack Two-Color Quantum Well Infrared Photodetector. *Appl. Phys. Lett.* **1997**, *70*, 859−861.
(35) Sarkar, S.; Basak, D. Understanding of Ultraviolet Photoresponse Properties of ZnO Nanorods: Effect of Nanorod's Size and Ambient. *ScienceJet* **2015**, *4*, 103.
(36) Panigrahi, S.; Basak, D. Morphology Driven Ultraviolet Photosensitivity in ZnO-CdS Composite. *J. Colloid Interface Sci.* **2011**, *364*, 10−17.
(37) Novotny, C. J.; Yu, E. T.; Yu, P. K. L. Inp Nanowire/Polymer Hybrid Photodiode. *Nano Lett.* **2008**, *8*, 775−779.
(38) Mridha, S.; Dutta, M.; Basak, D. Photoresponse of n-ZnO/p-Si Heterojunction Towards Ultraviolet/Visible Lights: Thickness Dependent Behavior. *J. Mater. Sci.: Mater. Electron.* **2009**, *20*, 376−379.
(39) Tak, Y.; Hong, S. J.; Lee, J. S.; Yong, K. Solution-Based Synthesis of a CdS Nanoparticle/ZnO Nanowire Heterostructure Array. *Cryst. Growth Des.* **2009**, *9*, 2627−2632.
(40) Zhang, G. H.; Jiang, S. L.; Lin, Y.; Ren, W. Z.; Cai, H. B.; Wu, Y. K.; Zhang, Q.; Pan, N.; Luo, Y.; Wang, X. P. Improving the Photovoltaic Performance of Solid-State ZnO/CdTe Core-Shell Nanorod Array Solar Cells Using a Thin CdS Interfacial Layer. *J. Mater. Chem. A* **2014**, *2*, 5675−5681.

DOI: 10.1021/acsami.5b03184
ACS Appl. Mater. Interfaces 2015, 7, 16322−16329

(41) Zhang, J. B.; Sun, C. Z.; Bai, S. L.; Luo, R. X.; Chen, A. F.; Sun, L. N.; Lin, Y. Interfacial Passivation of CdS Layer to CdSe Quantum Dots-Sensitized Electrodeposited ZnO Nanowire Thin Films. *Electrochim. Acta* **2013**, *106*, 121−126.

DOI: 10.1021/acsami.5b03184
ACS Appl. Mater. Interfaces 2015, 7, 16322−16329